ACS APPLIED MATERIALS & INTERFACES

Research Article

www.acsami.org

Fast Photoconductive Responses in Organometal Halide Perovskite Photodetectors

Fei Wang,[†] Jingjing Mei,[†,‡] Yunpeng Wang,*[,†] Ligong Zhang,[†] Haifeng Zhao,[†] and Dongxu Zhao*[,†]

[†]State Key Laboratory of Luminescence and Applications, Changchun Institute of Optics, Fine Mechanics and Physics, Chinese Academy of Sciences, 3888 Dongnanhu Road, Changchun 130021, People's Republic of China

[‡]University of Chinese Academy of Sciences, Beijing 100049, People's Republic of China

Supporting Information

ABSTRACT: Inorganic semiconductor-based photodetectors have been suffering from slow response speeds, which are caused by the persistent photoconductivity of semiconductor materials. For realizing high speed optoelectronic devices, the organometal halide perovskite thin films were applied onto the interdigitated (IDT) patterned Au electrodes, and symmetrical structured photoconductive detectors were achieved. The detectors were sensitive to the incident light signals, and the photocurrents of the devices were 2−3 orders of magnitude higher than dark currents. The responsivities of the devices could reach up to 55 mA W^{1-}. Most importantly, the detectors have a fast response time of less than 20 μs. The light and bias induced dipole rearrangement in organometal perovskite thin films has resulted in the instability of photocurrents, and Ag nanowires could quicken the process of dipole alignment and stabilize the photocurrents of the devices.

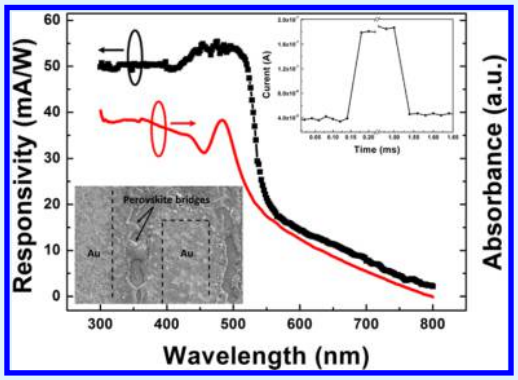

KEYWORDS: *organometal halide perovskites, photoconductive photodetectors, fast response, dipole alignment, Ag nanowires*

INTRODUCTION

Photodetectors, which can convert incident light signals into electric signals, are very important functional components for realizing a wide range of industrial and scientific applications including optical communication, environmental monitoring, day- and night-time surveillance, and chemical/biological sensing.[1,2] In the past few decades, most research attentions of photodetectors were paid to the inorganic semiconductor materials such as Si,[3−6] GaN,[7−10] and ZnO.[11−15] Also, both the photovoltaic and photoconductive devices have been intensively studied.[3−15] However, due to the persistent photoconductivity caused by the internal and surface deep-level defects,[11,15−18] the inorganic semiconductor-based photodetectors still suffer from slow responses of several seconds or longer,[3−15] which has greatly limited their applications in high-speed devices.

Recently, a group of organic/inorganic hybrid perovskite materials have attracted much attention due to their superb properties.[19−23] The metal halide octahedral cages in layered perovskite framework provide distinct advantages of ultrafast charge generation, high mobility, long charge carrier lifetime, and diffusion length;[24] meanwhile, the organic components offer a number of useful properties including structural diversity and capacity of solution processing. These interesting properties strongly suggest a huge potential of this class of materials for photodetector applications. And most importantly, the dominant intrinsic defects of organometal halide perovskites create only shallow-level defects, even with the defects inevitably formed during the low-cost solution-based process. Gap states within the band gap are not found.[25,26] So, the organometal halide perovskites could prevent the serious persistent photoconductivity of inorganic semiconductors, then realize the devices of fast response speeds. Yang et al.[1] have reported the sandwich structured photodetector with organic/inorganic hybrid perovskite materials as functional layer; the device presented a fast response speed and a high responsivity. But the use of electron transport layer (ETL) and hole transport layer (HTL) materials has increased the cost of the device, and the four-time spin-coating processes in their work have also added complexities to device fabrication. Photoconductive devices, which only need perovskite materials, metal electrodes, and one cycle of spin-coating, could be a facile way to accomplish perovskite photodetectors more easily and efficiently. Therefore, in this work, for achieving photoconductive photodectors with symmetrical structure, we used a simple but efficient approach to apply the organic/inorganic hybrid perovskite materials onto IDT patterned Au electrodes. The electrodes formed ohmic contacts with perovskite layer and the current of the device increased rapidly as soon as the incident light source was turned on. Perovskite based photoconductive photodectors with fast response speeds of less than 20 μs have been achieved.

Received: November 30, 2015
Accepted: January 12, 2016
Published: January 12, 2016

DOI: 10.1021/acsami.5b11621
ACS Appl. Mater. Interfaces 2016, 8, 2840−2846

EXPERIMENTAL SECTION

Methylammonium bromide (CH_3NH_3Br) and methylammonium iodide (CH_3NH_3I) used in this experiment were synthesized by the method mentioned elsewhere.[27−29] The perovskite precursor solutions were prepared by mixing CH_3NH_3Br or CH_3NH_3I with $PbCl_2$ in a 3:1 molar ratio in anhydrous *N*,*N*-dimethylformamide (DMF) to give the concentrations of 10, 20, and 30 wt %. Glass substrates (1 × 1 cm) were ultrasonically cleaned with acetone, ethanol, and deionized water for 15 min, respectively. Then, 50 nm thick Au thin films were deposited onto the glass substrates by a vacuum evaporation equipment under the pressure of 2×10^{-3} Pa, then optical lithography was applied to define the IDT contact patterns. The fingers of the Au contact electrodes were 500 μm long and 5 μm wide with 5 μm spacing. The $CH_3NH_3PbBr_{3-x}I_x$ and $CH_3NH_3PbI_3$ precursor solutions were spin-coated onto the substrates at 3500 rpm for 40 s and then annealed at 100 °C for 10 min.

The morphology of samples was investigated by the field-emission scanning electron microscopy (FESEM, Hitachi S-4800). The photoluminescence (PL) measurement was carried out with a JY-630 micro-Raman spectrometer by using the 325 nm line of a He−Cd laser as the excitation source, and the absorption spectra were carried out using a Shimadzu UV-3101 PC spectrophotometer. X-ray diffraction (XRD) patterns were collected with a Bruker D8 system. The typical *I*−*V* curves were measured by an Agilent B1500A semiconductor device analyzer, and the time-resolved photocurrent testing were carried out by using an optical chopper (EG&G 192) to turn on and turn off the light that illuminated on the device and using the semiconductor device analyzer and Agilent B2902A precision source/measure unit to record the time and corresponding photocurrent values. Commercial light-emitting diodes (LEDs, 400 , 470, and 525 nm) were served as excitation sources to carry out the *I*−*V* and time-resolved photocurrent characteristics of the device. The power densities of all LEDs were evaluated by Ophir PD300R-UV power meter and calibrated by adjusting the applied bias to achieve a similar intensity of 2 mW/cm^2. The *I*−*V* curves under different power densities were obtained under a laser diode (400 nm) and a Thorlabs linear variable ND filter.

RESULTS AND DISCUSSION

Figure 1 shows the FESEM images of the device. As can be seen from the figure, after spin-coating the mixed halide

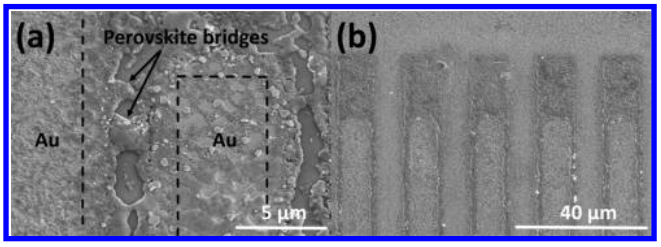

Figure 1. (a) SEM and (b) low-resolution SEM images of halide perovskite thin films on IDT contact patterns with the precursor concentration of 20 wt %.

perovskite precursor onto the ready-prepared IDT patterns, the Au electrodes are uniformly coated by $CH_3NH_3PbBr_{3-x}I_x$ material, and some crystal grains can be observed on the thin film, which indicates the formation of organometal halide perovskites. Figure S1 shows the XRD pattern of as-prepared $CH_3NH_3PbBr_{3-x}I_x$ films. There are only two main diffraction peaks located at 15.15 and 30.53°, which correspond to the (100) and (200) planes of the cubic phase perovskite.[2,30−32] The systematic shift of the diffraction pattern to higher angles can be attribute to the addition of bromide element, indicating a shrink of the unit cell with decreasing iodide fraction.[32] It is worth noting in Figure 1 that there are also some perovskite crystals formed between two electrodes, and the perovskite films on different figures of IDT patterns are connected together by this bridge-like perovskite crystals. The carriers could transmit from one electrode to neighboring electrode through the bridging perovskite, thus a simple photoconductive device has been achieved. Figure S3 shows the SEM images of the devices fabricated by 10 and 30 wt % precursor solutions. From the picture of 10 wt % device we could see the island-like perovskite crystals between two IDT fingers. Yet, the 30 wt % device presents the net-like crystal morphology, which spreads all over the IDT patterns. The size of bridging perovskites becomes bigger with the increasing concentration, and the shape of the bridging crystals transforms from islands to net morphology. Obviously, there are more bridging crystals in net-like perovskite than there are in island-like perovskite. The perovskite crystals on IDT patterns (Figure 1b and Figure S3a,b) all have rough surfaces, which are different from the ones applied on glass substrates in Figure S4.

Typical *I*−*V* characteristics of the detectors were carried out to reveal the electrical properties of the perovskite films. Figure 2a shows the *I*−*V* curves of the 20 wt % device in dark and under the illuminations of different wavelengths (400 nm, 470 and 525 nm). From the curves we can see that the perovskite has a high resistance in dark condition and the dark current is around 1 nA. Yet, when under illumination, the current increases by tens or hundreds times. The linear *I*−*V* curves

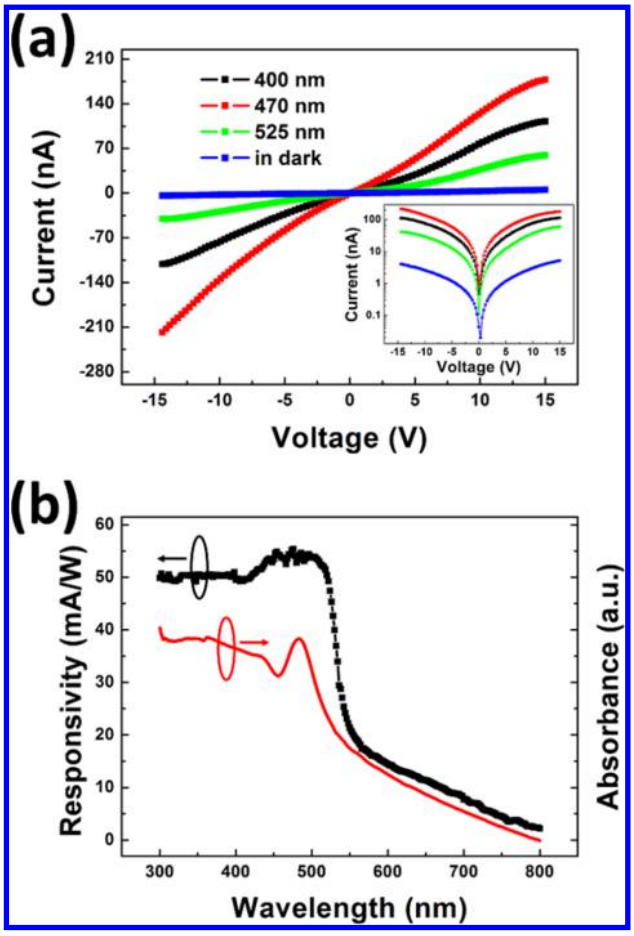

Figure 2. (a) Typical *I*−*V* characteristics of 20 wt % device, the inset of (a) presents the *I*−*V* curve on a natural logarithmic scale. (b) Room temperature responsivity and optical absorbance curves of the device.

DOI: 10.1021/acsami.5b11621
ACS Appl. Mater. Interfaces 2016, 8, 2840−2846

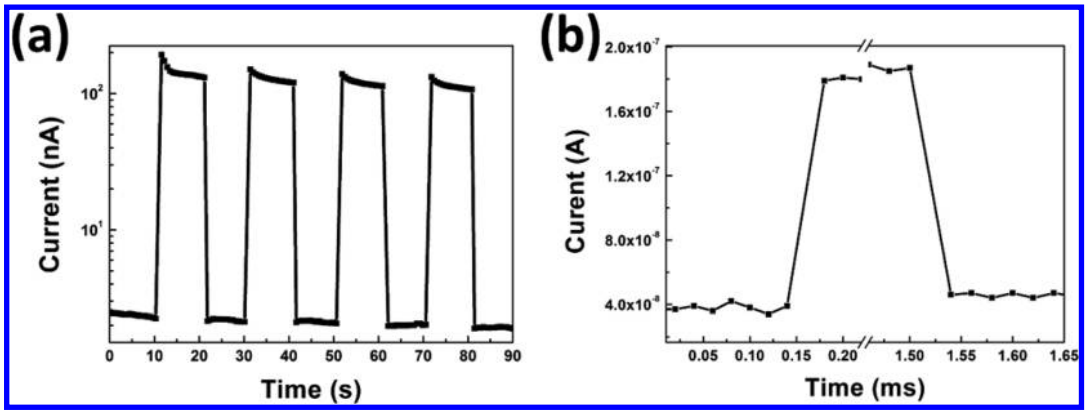

Figure 3. (a) Reproducible on/off switching of the 20 wt % device upon 400 nm light with a 10 s cycle illumination at a bias of 10 V. (b) Response of the device to pulsed light irradiation at frequencies of 800 Hz.

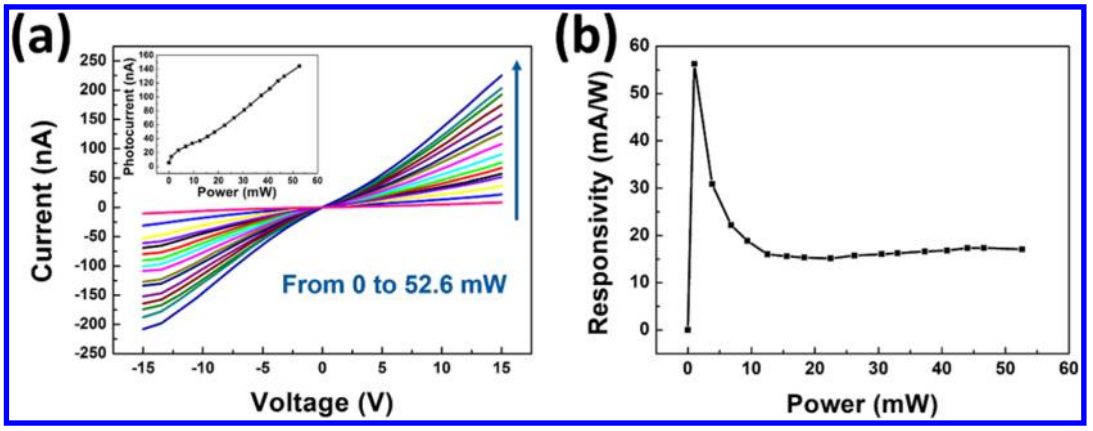

Figure 4. (a) Typical *I*–*V* characteristics of the 20 wt % device with different illumination power densities. (b) Responsivities of the device under different power densities.

imply that ohmic contacts have formed between Au and $CH_3NH_3PbBr_{3-x}I_x$, and the increase of the current means the device is sensitive to the incident photons. The photoinduced carriers can be separated and transferred to different electrodes under the effect of electric field, and the perovskite based photoconductive detector could be accomplished with this symmetrical device structure. However, under different wavelengths, the photocurrent values of the device are not the same. The highest photocurrent has been obtained under the illumination of 470 nm. With the applied bias of 10 V, the current could increase by 2 orders of magnitude. For revealing the correlation between the incident wavelengths and the responses of the device, the room temperature absorbance spectrum was evaluated and shown in Figure 2b. On the absorbance curve we can clearly see the exciton absorption peak located at 470 nm, and the absorbance of the wavelengths shorter than 470 nm are also strong. However, when the wavelength is longer than 500 nm, the absorbance of light decreases dramatically. The photocurrent value of a photodetector strongly depends on the light absorption of the material, so we see the lowest photocurrent under 525 nm illumination in Figure 2a. As a critical parameter to characterize the performance of photodetectors, the responsivities of the device have also been plotted at 10 V and shown in Figure 2b. The photoinduced carriers could only be collected and transferred between the IDT fingers, so the active area of the devices in this work to calculate the values of responsivity is defined as the product of the length and the width of IDT pattern. As can be seen from the figure, the responsivity curve is consistent with the absorption curve of the material, and the slight red-shift of the response edge can be attribute to the Stokes shift of the material. The peak of responsivity curve is also located at 470 nm and the responsivity value of the device can reach up to 55 mA W^{1-} under the illumination of 475 nm. The device fabricated by 10 wt % precursor solution has the photocurrent of several pA in Figure S5a, and there is no obvious responsivity can be observed from the spectrum of the device in Figure S5b, which may be attributed to the lack of bridging perovskites to absorb the photons and transmit the photo induced carriers. For the device fabricated from 30 wt % precursor, the photocurrent can reach up to about 100 nA, but the dark current is high too. It may be caused by the excessive bridging crystals. As the result, the responsivity of the device has not exceeded 25 mA/W, The 20 wt % device has the highest value of responsivity, so 20 wt % is the optimized concentration of precursor solution for fabricating organometal halide perovskite based photodetectors in this work.

The layered structure of organometal halide perovskite materials presents the properties of inorganic semiconductor materials and organic materials at the same time, and the cooperation of organic and inorganic components could greatly enhanced the properties for each other. They do not only have the inorganic material properties of ultrafast charge generation, high mobility and long charge carrier lifetime, but also enjoy the organic properties of easy fabrication and no deep-level defects. For organometal halide perovskites, dominant intrinsic

DOI: 10.1021/acsami.5b11621
ACS Appl. Mater. Interfaces 2016, 8, 2840–2846

defects create only shallow-level defects. Gap states within the band gap are not found,[25,26] which is rarely the case in conventional semiconductors such as Si, Ge, group III−V, and group II−VI semiconductors. For revealing the response speed, time-resolved photocurrent curves of the devices were investigated. As shown in Figure 3a, as soon as the light illuminated on the device is switched on, the current of the device raises drastically. In an extremely brief period the photocurrent has increased by 2 orders of magnitude. After several circles of "on" and "off" states, the device could also respond to the light signals with the same speed and the same current level, indicating the excellent reversibility and stability of the device. For further evaluating the response speed, we used a chopper with high frequencies to switch the light illuminated on the device. As can be seen in Figure 3b, the rise time and decay time of the device are all shorter than 20 μs. It should be mentioned that 20 μs has been limited by the present experimental setup. Yet, the device is still a fast one among kinds of semiconductor photodetectors.[3−15]

The relationship between the photocurrent and the light intensity is direct evidence of the stability of a photodetector under weak or strong signals. Therefore, we have explored the photosensitivity dependence of the device on light intensities. As shown in Figure 4a, the $I-V$ characteristics of the device have been evaluated under the illumination of 400 nm with different power intensities from 0 to 52.6 mW. The $I-V$ curves of the device raise gradually with increasing power intensities. The values of photocurrent are linearly proportional to the incident irradiation intensities within the range of 0−52.6 mW. That is, more photons could generate more photoinduced carriers in the device. No matter under weak or strong signals, the generation of the carriers in the device are constant and steady. The responsivity of the device reaches the highest value at the power of 1 mW, which was followed by a decay of the value. With the increasing power intensity over 10 mW, the responsivity maintains a steady value of 17.5 mA/W.

Organometal halide perovskites are a class of materials with the same tetragonal phases but different halide components and band gaps. For understanding whether the other hybrid perovskites could construct the symmetrical photoconductive detectors, we have also fabricated the device on the basis of $CH_3NH_3PbI_3$ material with the same method. Figure S2 exhibits the XRD pattern of the as-prepared $CH_3NH_3PbI_3$ films, the main diffraction peaks located at 14.15 and 28.45° that correspond to the (110) and (220) planes of the tetragonal phase perovskites. Figure S6a shows the $I-V$ curves of the device in dark and under the illumination of different wavelengths. The results indicate that ohmic contacts have formed between $CH_3NH_3PbI_3$ and Au electrodes, and the photocurrent values are still different under the illuminations of different wavelengths. The current could increase by 3 orders of magnitude under the light of 470 nm. Figure S6b shows the photoresponse characteristics of $CH_3NH_3PbI_3$ device under different wavelengths at the bias of 10 V. The peak of the responsivity curve is located at about 450 nm, but the edge of the curve has extended to 760 nm as compared to the $CH_3NH_3PbBr_{3-x}I_x$ device mentioned above. The usage of $CH_3NH_3PbI_3$ as the functional material could realize the broad spectral detection range from UV to the whole visible light. Also, Figure S7 and Figure S8 indicate that the $CH_3NH_3PbI_3$ device still has the fast response speed under the illumination of different wavelengths.

It is worth noting that on the time-resolved photocurrent curves of the devices, there are spikes followed by decays that can be observed when the light is turned on (Figure 3a and Figures S5c,f and S7). The photocurrent reaches the highest value at the very beginning of the illumination, then decays for many seconds to reach the steady state. It suggests that the perovskite material endures some kind of changes under the effects of illumination and bias. For revealing the cause of this phenomenon, time-resolved PL testing was performed. As can be seen in Figure 5, the intensity of PL peak is not so high at

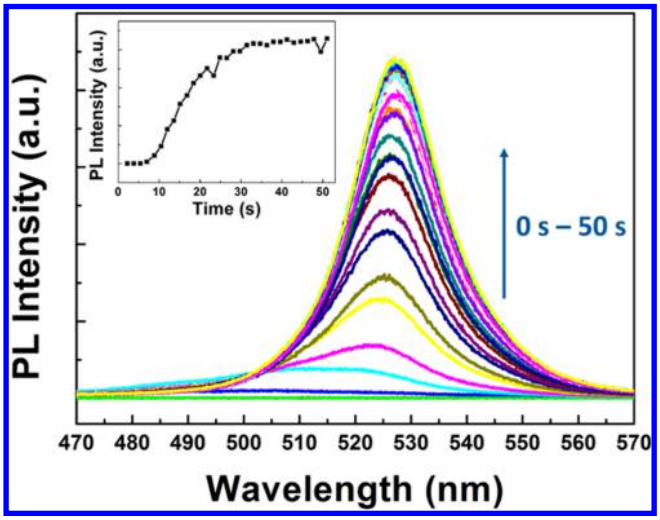

Figure 5. Room temperature PL spectra of halide perovskite thin film with the illumination time from 0 to 50 s and (inset) PL peak intensities with time.

the initial stage. With the increasing of illumination time, the peak gradually gets stronger. Additionally, the emission peak of the sample has a slight red shift as illumination time increases. It may originate from the dipole alignment that induced by the effect of external perturbations (light illumination or bias) in organometal halide perovskite materials.[33] For the room-temperature cubic phase perovskite, the methylammonium (MA) cations, which mainly interact with the inorganic cage by hydrogen bonding, exhibit a dynamic disorder state when there is no external perturbation.[34] Yet, under the light illumination, the MA cations may be less tightly bound in the excited state than in the ground state. They will rotate more freely and strongly orient along the crystallographic c axis to form an ordered structure with no octahedra tilting.[33] The transition between the proposed states is very slow, which could last for tens of seconds. So, in Figure 5, it takes more than 20 s to reach a steady state. Considering the spin−orbit coupling (SOC), the perovskite material endures a band gap reduction with the process of light-induced MA rearrangement.[33,35] That is why the PL peak red-shifts with the increasing illumination time.

To avoid the long duration to reach the stable photocurrent, we applied Ag nanowires in the device. Ag nanowires have been widely used in light harvesting systems,[36−39] it could enhance the interaction between light and materials, so they may play a part in speeding up the light-induced MA rearrangement in perovskite materials. The Ag nanowires used in this work were fabricated follow the method reported by Zaleski et al.[40] After the synthesis reaction, the Ag nanowires were centrifuged three times at 9000 rpm for 10 min to remove ethylene glycol, PVP, and other impurities. The precipitates of Ag nanowires were

DOI: 10.1021/acsami.5b11621
ACS Appl. Mater. Interfaces 2016, 8, 2840−2846

added into the 20 wt % perovskite precursor solution with the concentration of 0.2 wt %, then dispersed by an ultrasonic cleaner with short time of 15 s. The Ag nanowire has the diameter of 100−300 nm and the length of 3−6 μm, which is shown in Figure S9a. Figure 6a shows the time-resolved PL

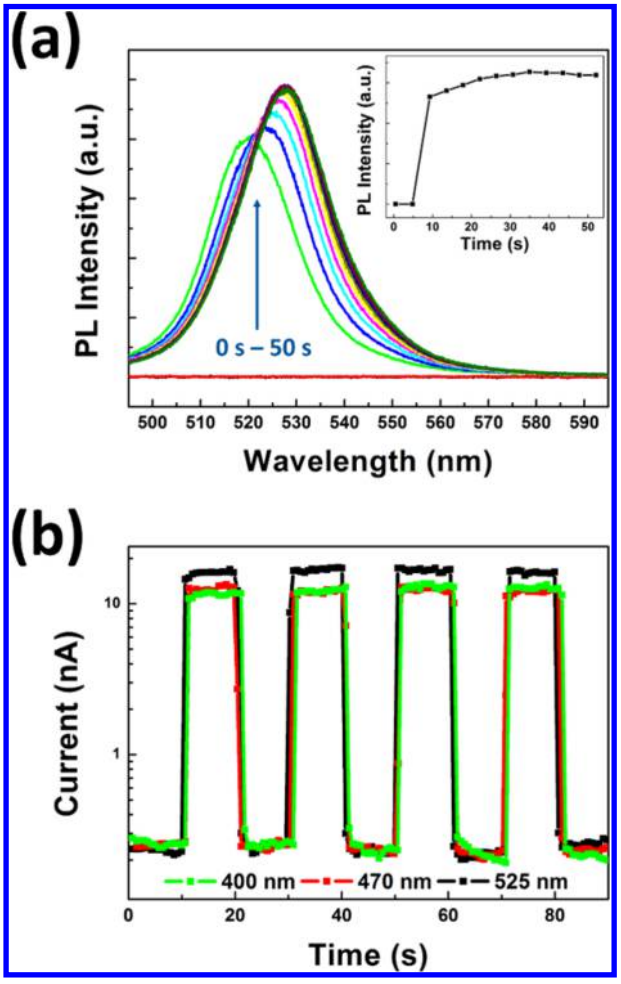

Figure 6. (a) Room temperature PL spectra of halide perovskite thin film combined with Ag nanowires from 0 to 50 s amd (inset) PL peak intensities with time. (b) Reproducible on/off switching of the Ag-nanowire assistant device upon different light illumination.

testing after the adding of Ag nanowires into the perovskite material, and the speed of the light mediated change from partially disordered to strongly ordered MA configurations becomes more faster. It reaches the steady PL value within 5 s, which means MA dipoles also reach the ordered orientation quickly. Figure 6b shows the time-resolved photocurrent curves of the Ag nanowire mediated device, the values of photocurrent reach the steady states as soon as the light illuminate on the device. Also, no spikes or decays could be observed on the curves. The addition of Ag nanowires may play two main roles: First, it has enhanced the light absorption of the perovskite materials. Figure S9b shows the absorbance spectrum of Ag assistant thin film, the absorption has been enhanced within the range from 300 to 550 nm, and the responsivity of the device has been enhanced as well. Second, the Ag nanowires could contribute to an intensity enhancement of the electronic field. The electronic field intensity between two IDT patterns can be defined as $E = U/d$, where E is the electronic field intensity, and U and d are the voltage and distance between two fingers, respectively. Ag is an excellent conductor of electricity, and when we add Ag nanowires into the perovskite materials, the Ag nanowires can connect to the IDT pattern, then shorten the distance d. With the same voltage U, the electronic field intensity E has been enhanced. The MA cations can more freely rotate under the action of the larger applied electric field,[33] so the light-induced MA rearrangement in the perovskite materials has been quickened.

Considering the above analyses, we could conclude that the ordered arrangement of MA cations in perovskite materials can contribute to stronger PL intensities and wider band gaps. So during the light induced rearrangement process of MA cations, the PL intensity gradually becomes higher, and the PL peak has red-shifted slightly. But in the photodetecting process with the combined effect of light illumination and electronic field, the device reaches the highest photocurrent first, then followed by a decay of the value. The both hysteresis of decay and direct rise cases under illumination and electronic field have been observed by other researchers.[33,41,42] Even with the same structure, the responses are sample specific. The different two cases could be observed in separately fabricated devices. The two opposite cases may be caused by the different of highly subtle parameters during the deposition procedure, which could control the specific structure or orientation of the polycrystalline film.[43] Under the combined effect of illumination and electronic field, the collective alignments of the MA dipoles are different with the specific structures or orientations.[33,41] So, in some devices, the photocurrent decreases, while other devices experience an increase.

CONCLUSION

In summary, by applying the organometal halide perovskite thin films onto the IDT patterned Au electrodes, symmetrical structured photoconductive detectors were achieved. The formation of perovskite bridges between two fingers of IDT patterns connected the electrodes together. The detectors were sensitive to the incident light signals, and the photocurrent values of the devices were different when illuminated by light of different wavelengths. The photocurrents of the devices were 2−3 orders of magnitude higher than dark currents, and the responsivities could reach up to 55 mA W^{1-}. Most importantly, the detectors have a fast response time of less than 20 μs. The illumination and electronic-field-induced dipole alignment resulted in a decay of the photocurrent, and the introduction of Ag nanowires increased the rate of the rearrangement process. The methods and discussions mentioned here not only prove that the organometal halide perovskite could be applied to symmetrical structured photoconductive detectors but also provide a kind of photoelectric devices for the fast operating systems.

ASSOCIATED CONTENT

Supporting Information

The Supporting Information is available free of charge on the ACS Publications website at DOI: 10.1021/acsami.5b11621.

XRD patterns of perovskite thin films; SEM images, typical $I-V$ characteristics, room temperature responsivity, and reproducible on/off switching curves of the devices with different precursor concentrations; typical $I-V$ characteristics, room temperature responsivity, optical absorbance, and reproducible on/off switching

DOI: 10.1021/acsami.5b11621
ACS Appl. Mater. Interfaces 2016, 8, 2840−2846

of the $CH_3NH_3PbI_3$device; and room temperature responsivity and optical absorbance curves of Ag-nanowire assistant thin film. (PDF)

AUTHOR INFORMATION

Corresponding Authors

*E-mail: wangyunpeng@ciomp.ac.cn.
*E-mail: zhaodx@ciomp.ac.cn. Tel: +86-431-86708227.

Notes

The authors declare no competing financial interest.

ACKNOWLEDGMENTS

This work was supported by the National Basic Research Program of China (973 Program) under Grant No. 2011CB302004, the National Natural Science Foundation of China under Grant No. 11504367.

REFERENCES

(1) Dou, L.; Yang, Y.; You, J.; Hong, Z.; Chang, W. H.; Li, G.; Yang, Y. Solution-Processed Hybrid Perovskite Photodetectors with High Detectivity. *Nat. Commun.* **2014**, *5*, 5404.

(2) Hu, X.; Zhang, X.; Liang, L.; Bao, J.; Li, S.; Yang, W.; Xie, Y. High-Performance Flexible Broadband Photodetector Based on Organolead Halide Perovskite. *Adv. Funct. Mater.* **2014**, *24*, 7373−7380.

(3) Wang, L.; Jie, J.; Shao, Z.; Zhang, Q.; Zhang, X.; Wang, Y.; Sun, Z.; Lee, S. T. MoS_2/Si Heterojunction with Vertically Standing Layered Structure for Ultrafast, High-Detectivity, Self-Driven Visible-Near Infrared Photodetectors. *Adv. Funct. Mater.* **2015**, *25*, 2910−2919.

(4) Das, K.; Mukherjee, S.; Manna, S.; Ray, S. K.; Raychaudhuri, A. K. Single Si Nanowire (diameter # 100 nm) Based Polarization Sensitive Near-Infrared Photodetector with Ultra-High Responsivity. *Nanoscale* **2014**, *6*, 11232−11239.

(5) Hong, Q.; Cao, Y.; Xu, J.; Lu, H.; He, J.; Sun, J. L. Self-Powered Ultrafast Broadband Photodetector Based on p−n Heterojunctions of CuO/Si Nanowire Array. *ACS Appl. Mater. Interfaces* **2014**, *6*, 20887−20894.

(6) Xie, C.; Li, F.; Zeng, L.; Luo, L.; Wang, L.; Wu, C.; Jie, J. Surface Charge Transfer Induced p-CdS Nanoribbon/n-Si Heterojunctions as Fast-Speed Self-Driven Photodetectors. *J. Mater. Chem. C* **2015**, *3*, 6307−6313.

(7) Lin, F.; Chen, S. W.; Meng, J.; Tse, G.; Fu, X. W.; Xu, F. J.; Shen, B.; Liao, Z. M.; Yu, D. P. Graphene/GaN Diodes for Ultraviolet and Visible Photodetectors. *Appl. Phys. Lett.* **2014**, *105*, 073103.

(8) Rigutti, L.; Tchernycheva, M.; De Luna Bugallo, A.; Jacopin, G.; Julien, F. H.; Zagonel, L. F.; March, K.; Stephan, O.; Kociak, M.; Songmuang, R. Ultraviolet Photodetector Based on GaN/AlN Quantum Disks in a Single Nanowire. *Nano Lett.* **2010**, *10*, 2939−2943.

(9) Wu, H.; Sun, Y.; Lin, D.; Zhang, R.; Zhang, C.; Pan, W. GaN Nanofibers Based on Electrospinning: Facile Synthesis, Controlled Assembly, Precise Doping, and Application as High Performance UV Photodetector. *Adv. Mater.* **2009**, *21*, 227−231.

(10) Zhao, Z. M.; Jiang, R. L.; Chen, P.; Xi, D. J.; Luo, Z. Y.; Zhang, R.; Shen, B.; Chen, Z. Z.; Zheng, Y. D. Metal−Semiconductor−Metal GaN Ultraviolet Photodetectors on Si(111). *Appl. Phys. Lett.* **2000**, *77*, 444−446.

(11) Soci, C.; Zhang, A.; Xiang, B.; Dayeh, S. A.; Aplin, D. P. R.; Park, J.; Bao, X. Y.; Lo, Y. H.; Wang, D. ZnO Nanowire UV Photodetectors with High Internal Gain. *Nano Lett.* **2007**, *7*, 1003−1009.

(12) Chen, M.; Hu, L.; Xu, J.; Liao, M.; Wu, L.; Fang, X. ZnO Hollow-Sphere Nanofilm-Based High-Performance and Low-Cost Photodetector. *Small* **2011**, *7*, 2449−2453.

(13) Yang, Q.; Guo, X.; Wang, W.; Zhang, Y.; Xu, S.; Lien, D. H.; Wang, Z. L. Enhancing Sensitivity of a Single ZnO Micro-/Nanowire Photodetector by Piezo-Phototronic Effect. *ACS Nano* **2010**, *4*, 6285−6291.

(14) Hu, L.; Yan, J.; Liao, M.; Xiang, H.; Gong, X.; Zhang, L.; Fang, X. An Optimized Ultraviolet-A Light Photodetector with Wide-Range Photoresponse Based on ZnS/ZnO Biaxial Nanobelt. *Adv. Mater.* **2012**, *24*, 2305−2309.

(15) Ali Raza, S. R.; Lee, Y. T.; Hosseini Shokouh, S. H.; Ha, R.; Choi, H.-J.; Im, S. A. ZnO Nanowire-based Photo-Inverter with Pulse-Induced Fast Recovery. *Nanoscale* **2013**, *5*, 10829−10834.

(16) Qiu, C. H.; Pankove, J. I. Deep Levels and Persistent Photoconductivity in GaN Thin Films. *Appl. Phys. Lett.* **1997**, *70*, 1983−1985.

(17) Reddy, C. V.; Balakrishnan, K.; Okumura, H.; Yoshida, S. The Origin of Persistent Photoconductivity and Its Relationship with Yellow Luminescence in Molecular Beam Epitaxy Grown Undoped GaN. *Appl. Phys. Lett.* **1998**, *73*, 244−246.

(18) Jin, Y. Z.; Wang, J. P.; Sun, B. Q.; Blakesley, J. C.; Greenham, N. C. Solution-Processed Ultraviolet Photodetectors Based on Colloidal ZnO Nanoparticles. *Nano Lett.* **2008**, *8*, 1649−1653.

(19) Yang, Y.; Yan, Y.; Yang, M.; Choi, S.; Zhu, K.; Luther, J. M.; Beard, M. C. Low Surface Recombination Velocity in Solution-Grown $CH_3NH_3PbBr_3$ Perovskite Single Crystal. *Nat. Commun.* **2015**, *6*, 7961.

(20) Kojima, A.; Teshima, K.; Shirai, Y.; Miyasaka, T. Organometal Halide Perovskites as Visible-Light Sensitizers for Photovoltaic Cells. *J. Am. Chem. Soc.* **2009**, *131*, 6050−6051.

(21) Lee, M. M.; Teuscher, J.; Miyasaka, T.; Murakami, T. N.; Snaith, H. J. Efficient Hybrid Solar Cells Based on Meso-Superstructured Organometal Halide Perovskites. *Science* **2012**, *338*, 643−647.

(22) Burschka, J.; Pellet, N.; Moon, S. J.; Humphry-Baker, R.; Gao, P.; Nazeeruddin, M. K.; Gratzel, M. Sequential Deposition as a Route to High-Performance Perovskite-Sensitized Solar Cells. *Nature* **2013**, *499*, 316−319.

(23) Liu, M.; Johnston, M. B.; Snaith, H. J. Efficient Planar Heterojunction Perovskite Solar Cells by Vapour Deposition. *Nature* **2013**, *501*, 395−398.

(24) Ponseca, J. C. S.; Savenije, T. J.; Abdellah, M.; Zheng, K.; Yartsev, A.; Pascher, T.; Harlang, T.; Chabera, P.; Pullerits, T.; Stepanov, A.; Wolf, J. P.; Sundström, V. Organometal Halide Perovskite Solar Cell Materials Rationalized: Ultrafast Charge Generation, High and Microsecond-Long Balanced Mobilities, and Slow Recombination. *J. Am. Chem. Soc.* **2014**, *136*, 5189−5192.

(25) Kim, J.; Lee, S. H.; Lee, J. H.; Hong, K. H. The Role of Intrinsic Defects in Methylammonium Lead Iodide Perovskite. *J. Phys. Chem. Lett.* **2014**, *5*, 1312−1317.

(26) Yin, W. J.; Shi, T.; Yan, Y. Unusual defect physics in $CH_3NH_3PbI_3$ perovskite solar cell absorber. *Appl. Phys. Lett.* **2014**, *104*, 063903.

(27) Tan, Z. K.; Moghaddam, R. S.; Lai, M. L.; Docampo, P.; Higler, R.; Deschler, F.; Price, M.; Sadhanala, A.; Pazos, L. M.; Credgington, D.; Hanusch, F.; Bein, T.; Snaith, H. J.; Friend, R. H. Bright Light-Emitting Diodes Based on Organometal Halide Perovskite. *Nat. Nanotechnol.* **2014**, *9*, 687−692.

(28) Im, J. H.; Jang, I. H.; Pellet, N.; Grätzel, M.; Park, N. G. Growth of $CH_3NH_3PbI_3$ Cuboids with Controlled Size for High-Efficiency Perovskite Solar Cells. *Nat. Nanotechnol.* **2014**, *9*, 927−932.

(29) Xing, G.; Mathews, N.; Lim, S. S.; Yantara, N.; Liu, X.; Sabba, D.; Grätzel, M.; Mhaisalkar, S.; Sum, T. C. Low-Temperature Solution-Processed Wavelength-Tunable Perovskites for Lasing. *Nat. Mater.* **2014**, *13*, 476−480.

(30) Zhang, M.; Yu, H.; Lyu, M.; Wang, Q.; Yun, J. H.; Wang, L. Composition-Dependent Photoluminescence Intensity and Prolonged Recombination Lifetime of Perovskite $CH_3NH_3PbBr_{3-x}Cl_x$ Films. *Chem. Commun.* **2014**, *50*, 11727−11730.

(31) Christians, J. A.; Miranda Herrera, P. A. M.; Kamat, P. V. Transformation of the Excited State and Photovoltaic Efficiency of

DOI: 10.1021/acsami.5b11621
ACS Appl. Mater. Interfaces 2016, 8, 2840−2846

$CH_3NH_3PbI_3$ Perovskite upon Controlled Exposure to Humidified Air. *J. Am. Chem. Soc.* **2015**, *137*, 1530−1538.
(32) Sadhanala, A.; Deschler, F.; Thomas, T. H.; Dutton, S. E.; Goedel, K. C.; Hanusch, F. C.; Lai, M. L.; Steiner, U.; Bein, T.; Docampo, P.; Cahen, D.; Friend, R. H. Preparation of Single-Phase Films of $CH_3NH_3Pb(I_{1-x}Br_x)_3$ with Sharp Optical Band Edges. *J. Phys. Chem. Lett.* **2014**, *5*, 2501−2505.
(33) Gottesman, R.; Haltzi, E.; Gouda, L.; Tirosh, S.; Bouhadana, Y.; Zaban, A.; Mosconi, E; De Angelis, F. Extremely Slow Photoconductivity Response of $CH_3NH_3PbI_3$ Perovskites Suggesting Structural Changes under Working Conditions. *J. Phys. Chem. Lett.* **2014**, *5*, 2662−2669.
(34) Poglitsch, A.; Weber, D. Dynamic Disorder in Methylammoniumtrihalogenoplumbates (II) Observed by Millimeter-Wave Spectroscopy. *J. Chem. Phys.* **1987**, *87*, 6373−6378.
(35) Amat, A.; Mosconi, E.; Ronca, E.; Quarti, C.; Umari, P.; Nazeeruddin, M. K.; Graetzel, M.; De Angelis, F. Cation-Induced Band-Gap Tuning in Organohalide Perovskites: Interplay of Spin−Orbit Coupling and Octahedra Tilting. *Nano Lett.* **2014**, *14*, 3608−3616.
(36) Schider, G.; Krenn, J. R.; Hohenau, A.; Ditlbacher, H.; Leitner, A.; Aussenegg, F. R.; Schaich, W. L.; Puscasu, I; Monacelli, B; Boreman, G. Plasmon Dispersion Relation of Au and Ag Nanowires. *Phys. Rev. B: Condens. Matter Mater. Phys.* **2003**, *68*, 155427.
(37) Cheng, B.; Le, Y.; Yu, J. Preparation and Enhanced Photocatalytic Activity of $Ag@TiO_2$ Core−Shell Nanocomposite Nanowires. *J. Hazard. Mater.* **2010**, *177*, 971−977.
(38) Feng, W.; Sun, L. D.; Yan, C. H. Ag Nanowires Enhanced Upconversion Emission of $NaYF_4$:Yb,Er Nanocrystals via a Direct Assembly Method. *Chem. Commun.* **2009**, *29*, 4393−4395.
(39) Bi, Y.; Hu, H.; Ouyang, S.; Jiao, Z.; Lu, G.; Ye, J. Selective Growth of Ag_3PO_4 Submicro-cubes on Ag Nanowires to Fabricate Necklace-Like Heterostructures for Photocatalytic Applications. *J. Mater. Chem.* **2012**, *22*, 14847−14850.
(40) Gou, L.; Chipara, M.; Zaleski, J. M. Convenient, Rapid Synthesis of Ag Nanowires. *Chem. Mater.* **2007**, *19*, 1755−1760.
(41) Snaith, H. J.; Abate, A.; Ball, J. M.; Eperon, G. E.; Leijtens, T.; Noel, N. K.; Stranks, S. D.; Wang, J. T.-W.; Wojciechowski, K.; Zhang, W. Anomalous Hysteresis in Perovskite Solar Cells. *J. Phys. Chem. Lett.* **2014**, *5*, 1511−1515.
(42) Sanchez, R. S.; Gonzalez-Pedro, V.; Lee, J.-W.; Park, N.-G.; Kang, Y. S.; Mora-Sero, I.; Bisquert, J. Slow Dynamic Processes in Lead Halide Perovskite Solar Cells. Characteristic Times and Hysteresis. *J. Phys. Chem. Lett.* **2014**, *5*, 2357−2363.
(43) Choi, J. J.; Yang, X.; Norman, Z. M.; Billinge, S. J. L.; Owen, J. S. Structure of Methylammonium Lead Iodide Within Mesoporous Titanium Dioxide: Active Material in High-Performance Perovskite Solar Cells. *Nano Lett.* **2014**, *14*, 127−133.

DOI: 10.1021/acsami.5b11621
ACS Appl. Mater. Interfaces 2016, 8, 2840−2846